Experimental Investigation of a Cavity-Mode Resonator Using a Micromachined Two-Dimensional Silicon Phononic Crystal in a Square Lattice

Nan Wang, J. M. Tsai, Fu-Li Hsiao, B. W. Soon, Dim-Lee Kwong, Moorthi Palaniapan, and Chengkuo Lee

***Abstract*—A 2-D silicon phononic crystal (PnC) slab of a square array of cylindrical air holes in a 10-μm-thick freestanding silicon plate with line defects is characterized as a cavity-mode PnC resonator. A piezoelectric aluminum nitride (AlN) film is employed as the interdigital transducers to transmit and detect acoustic waves, thus making the whole microfabrication process CMOS compatible. Both the band structure of the PnC and the transmission spectrum of the proposed PnC resonator are analyzed and optimized using finite-element method. The measured quality factor (Q factor) of the microfabricated PnC resonator is over 1000 at its resonant frequency of 152.46 MHz. The proposed PnC resonator shows promising acoustic resonance characteristics for radio-frequency communications and sensing applications.**

***Index Terms*—Cavity mode, CMOS compatible, phononic crystal (PnC), resonator.**

I. Introduction

ONE of the key components in radio-frequency (RF) communication devices is the frequency reference oscillator. Silicon-based integrated micromechanical oscillators are gaining more research interest because of their advantage of monolithic integration with integrated circuits [1]. Two types of microresonator technologies, namely, capacitive- and piezoelectric-based approaches, have been investigated comprehensively. However, there is a tradeoff for these two types of devices, i.e., the tradeoff between Q factor and motional impedance. For silicon micromechanical reference oscillators using capacitive MEMS resonators, researchers have already demonstrated a frequency–quality-factor $(f–Q)$ product as high as 2×10^{13} [2]. However, the motional impedance is also very high due to weak capacitive electroacoustic coupling. On the other hand, although the motional impedance of piezoelectric-based microresonators can be below 50 Ω, the Q factor cannot be very high due to high loss in the piezoelectric materials [3].

Two-dimensional silicon phononic crystal (PnC) slabs have been experimentally characterized as phononic bandgap structures, where scattering inclusions, e.g., air holes, arranged periodically in a homogeneous host material, e.g., silicon, enable certain frequencies to be completely reflected by the phononic structure [4]–[6]. In addition to freestanding PnC slabs of periodically arranged air holes, various PnC bandgap structures, such as cylindrical rods inside air holes [7], [8] and cylindrical rods embedded inside the membrane [9], as well as inverse acoustic bandgap structures [10], have been studied because the 2-D nature of PnC slabs guides the acoustic wave within the slab with better confinement of elastic energy. Researchers have also demonstrated the PnC slabs which can be operated in gigahertz frequencies [11], [12], providing PnCs a promising application in RF communications.

When defects are created in the PnC structure, devices of various functionalities like waveguides and resonators have been reported [13]–[15]. A PnC resonator was proposed as a potential candidate to overcome the aforementioned tradeoff between Q factor and motional impedance as a PnC can store elastic energy in a microcavity made of high-Q materials such as silicon [16]. In this letter, we fabricate and characterize a cavity-mode PnC resonator based on a 2-D PnC of a square lattice. Both the band structure of the PnC and the transmission spectrum of the designed PnC resonator are analyzed using finite-element method (FEM), while measurement results of the resonant behavior of the PnC resonator with high-Q resonant peak in the hundred-megahertz range are presented.

II. Modeling and Design

The studies of the propagation of bulk waves in 2-D PnCs start from bandgap analysis in finite structures based on a FEM approach, i.e., COMSOL Multiphysics software. A unit cell of the 2-D PnC slab is constructed for the first step of the FEM as shown in the inset in Fig. 1(a). Subdomain settings are then applied to simulate the structure of air holes in the

Manuscript received February 12, 2011; revised March 20, 2011; accepted March 23, 2011. Date of publication May 5, 2011; date of current version May 25, 2011. This work was supported by SERC of the Agency for Science, Technology and Research under Grant 1021010022. The review of this letter was arranged by Editor W. T. Ng.

N. Wang and B. W. Soon are with the Institute of Microelectronics, Agency for Science, Technology and Research, Singapore 117685, and also with the Department of Electrical and Computer Engineering, National University of Singapore, Singapore 117576.

J. M. Tsai and D.-L. Kwong are with the Institute of Microelectronics, Agency for Science, Technology and Research, Singapore 117685.

F.-L. Hsiao is with the Department of Electrical and Computer Engineering, National University of Singapore, Singapore 117576, and also with the Graduate Institute of Photonics, National Changhua University of Education, Changhua 500, Taiwan.

M. Palaniapan and C. Lee are with the Department of Electrical and Computer Engineering, National University of Singapore, Singapore 117576 (e-mail: elelc@nus.edu.sg).

Color versions of one or more of the figures in this letter are available online at http://ieeexplore.ieee.org.

Digital Object Identifier 10.1109/LED.2011.2136311

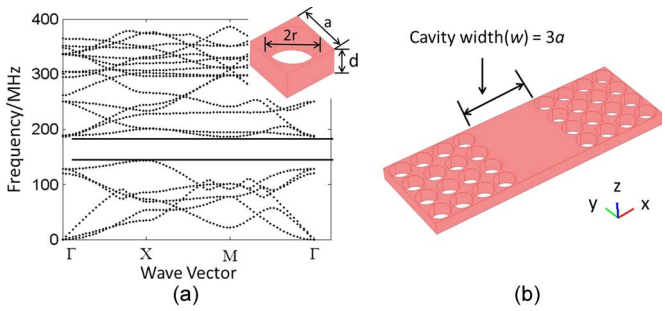

Fig. 1. (a) Band structure of the PnC with $d = 10\ \mu$m, $r = 8.18\ \mu$m, and $a = 18.18\ \mu$m, which gives $r/a = 0.45$ and $d/a = 0.55$. A unit cell of the structure is shown in the inset. (b) Schematic drawing of the PnC cavity-mode resonator formed by removing three rows of air holes (cavity width $w = 3a$) at the center.

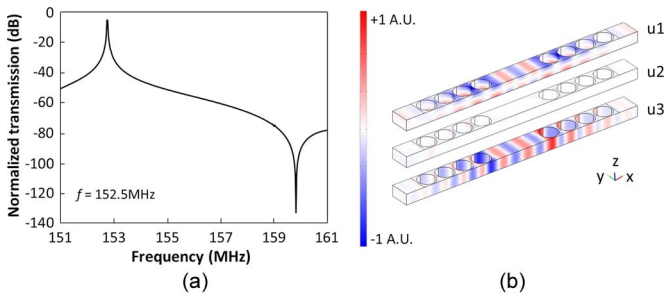

Fig. 2. (a) Simulated transmission spectrum of the designed PnC resonator. (b) Simulated mode profiles of displacement of the PnC resonator.

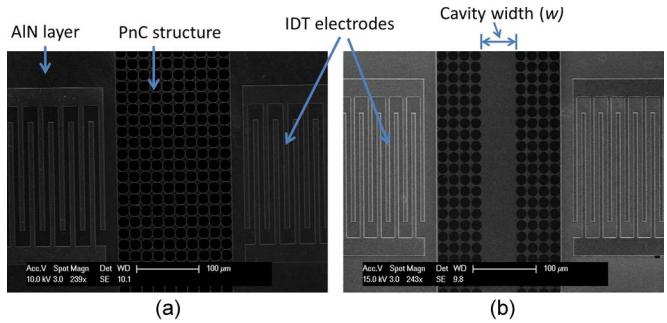

Fig. 3. SEM images of (a) the optimized PnC structure (b) the microfabricated PnC resonator. IDT electrodes are on the two sides of the phononic structure.

Si background. Zero charge/symmetry is applied on the electric boundary condition, and periodic boundary conditions are applied along the x- and y-directions. Lastly, we combine all the eigenfrequencies computed by the eigenfrequency solver to generate the band structure. As shown in the schematic drawing [inset in Fig. 1(a)], a is the lattice constant referring to the distance between the centers of two adjacent holes, d is the thickness of the PnC slab, and r is the radius of the air holes. For the bandgap calculation, we use $r/a = 0.45$ and $d/a = 0.55$ according to the theoretical optimization done in [5] and the limitation of microfabrication capability. The calculated band structure shown in Fig. 1(a) has a stopband of 143.3 MHz $> f >$ 186.3 MHz, which renders the gap-to-midgap frequency ratio to be 26.1%.

The confinement and guiding of acoustic energy through the use of defect inclusions in PnC structures are also analyzed using FEM. Here, we design a PnC cavity-mode resonator formed by removing three rows of air holes (cavity width $w = 3a$) at the center [Fig. 1(b)] from the 2-D PnC structure. To explore the resonant behavior of the designed PnC resonator structure, FEM is done using COMSOL Multiphysics software. Using the model constructed in Fig. 1(b), periodic boundary conditions are first applied along the y-direction. A frequency response solver is then used to obtain the transmission spectrum and the mode profiles of displacement in the x-, y-, and z-directions of the designed PnC resonator under its resonant frequency. The transmission spectrum in Fig. 2(a) shows that the resonant frequency of the PnC resonator is 152.5 MHz and the estimated Q factor is 10 000. As the elastic waves in the silicon plate propagate by the interactions among the silicon atoms when they are displaced from their equilibrium positions, the energy stored in any solid structure is then associated with the displacements of the silicon atoms within the silicon plate. Thus, by analyzing the displacements of all the silicon atoms within the silicon plate (mode profiles of displacement), we can get information about the energy distribution along the structure. Fig. 2(b) shows the mode profiles of displacement of the designed PnC resonator at its resonant frequency, i.e., 152.5 MHz. $u1$, $u2$, and $u3$ represent the displacement vector components in the x-, y-, and z-directions, respectively. The color bar indicates the amplitude of displacements in an arbitrary unit. We observe that, for our designed PnC resonator, the displacement vector components in the x- and z-directions are concentrated at the central defect region. With the advantage of good confinement of the elastic energy by the phononic structure surrounding the central defect region in the proposed design, a high Q factor is expected to be achieved.

III. Microfabrication

To realize the 2-D PnC slab structures, a silicon-on-insulator (SOI) wafer with a 10-μm device layer was first deposited with a 1-μm AlN layer and a 0.5-μm top Al electrode layer. The deposited AlN layer and top Al electrode were patterned subsequently using reactive-ion etching (RIE) to form the interdigital transducer (IDT) for generation and detection of the input and output of the acoustic waves. Cylindrical air holes in the square lattice arrangement were created on the silicon device layer by deep RIE (DRIE) to form PnC structures. Lastly, the 2-D silicon PnC slab becomes a freestanding plate which was released from the SOI substrate by using back-side DRIE for the silicon handle wafer portion and RIE for the silicon oxide insulator layer, i.e., buried oxide layer. Fig. 3(a) shows the microfabricated PnC structure after bandgap optimization. Fig. 3(b) shows the microfabricated PnC resonator. IDT electrodes are formed by an Al film on the two sides of the PnC structure.

IV. Device Characterization

To experimentally characterize the microfabricated PnC devices, an Agilent E8364B network analyzer (short-open-load-through calibrated) was used to measure the transmission spectrum against frequency via the IDT electrodes on the two sides of the PnC devices. Due to the piezoelectric properties of the AlN film, acoustic waves were launched toward the PnC

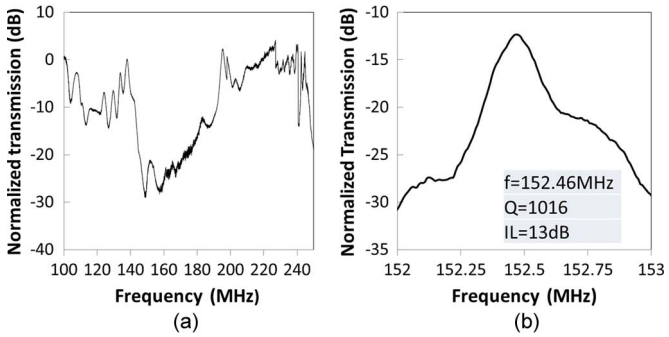

Fig. 4. Measured transmission spectrum of (a) the optimized PnC structure and (b) the microfabricated PnC resonator.

structure when an ac signal was applied on the IDT of the input port. The transmission through the PnC structure was picked up by the IDT of the output port. We then extracted the S_{21} parameter which is essentially the transmission of acoustic waves after the interaction with the PnC structure. A freestanding silicon slab without any PnC structure and with the same length is characterized by the same measurement setup such that the wave propagation of the tested PnC devices is normalized with respect to the transmission of the freestanding silicon slab in the same frequency range.

The measured transmission spectrum in Fig. 4(a) shows that the microfabricated PnC structure has a bandgap of 140 MHz $<$ f $>$ 195 MHz, which agrees quite well with the simulated data shown in Fig. 1(a). Fig. 4(b) shows that the microfabricated PnC cavity-mode resonator has a resonant frequency of 152.46 MHz, a Q factor of 1016, and an insertion loss (IL) of 13 dB. The tested resonant frequency also agrees quite well with the simulated data. The slight deviation of the measured resonant frequency could be due to deviation of the hole size and lattice constant introduced in the microfabrication step. The relatively high Q factor obtained is also expected because, from the modeling results on the mode profiles of displacement [Fig. 2(b)], we observe that the displacement vector components in the x- and z-directions are concentrated at the central defect region, leading to good confinement of the elastic energy by the PnC resonator. However, the tested Q factor deviates from the simulated value by an order of magnitude. This is because, as the periodic boundary conditions were applied in the simulation, scattering loss, which is a major source of energy loss, is not considered. Moreover, the achieved $(f–Q)$ product is as high as 1.5×10^{11}. From the obtained IL in the transmission spectrum, the value of the equivalent motional impedance can be extracted by (1) when the resonator is directly connected to the 50-Ω terminations of the network analyzer [17]

$$R_{\mathrm{eq}} = 50 \times 10^{IL/20}. \tag{1}$$

Thus, the characterized PnC resonator of the square lattice is a very promising resonator candidate for wireless communications in the hundred-megahertz range since the PnC resonator provides large Q factor in air while the motional impedance is low. The further optimization of the PnC resonator could lead for practical applications to RF communications in the gigahertz range.

V. Conclusion

In this letter, we have reported modeling and experimental data of a PnC cavity-mode resonator based on a 2-D phononic structure of a square lattice. The designed PnC resonator was realized from a microfabricated silicon freestanding plate. We characterized the resonator in terms of its resonant frequency, Q factor, and IL. The achieved $(f–Q)$ product is as high as 1.5×10^{11}. It demonstrates its promise in hundred-megahertz-range applications for wireless communications.

References

[1] H. M. Lavasani, R. Abdolvand, and F. Ayazi, "A 500 MHz low phase-noise AlN-on-silicon reference oscillator," in *Proc. IEEE CICC*, 2007, pp. 599–602.

[2] C. T. C. Nguyen, "MEMS technology for timing and frequency control," *IEEE Trans. Ultrason., Ferroelectr., Freq. Control*, vol. 54, no. 2, pp. 251–270, Feb. 2007.

[3] G. Piazza, P. J. Stephanou, and A. P. Pisano, "Single-chip multiple-frequency AlN MEMS filters based on contour-mode piezoelectric resonators," *J. Microelectromech. Syst.*, vol. 16, no. 2, pp. 319–328, Apr. 2007.

[4] S. Mohammadi, A. A. Eftekhar, A. Khelif, W. D. Hunt, and A. Adibi, "Evidence of large high frequency complete phononic band gaps in silicon phononic crystal plates," *Appl. Phys. Lett.*, vol. 92, no. 22, pp. 221905-1–221905-3, Jun. 2008.

[5] S. Mohammadi, A. A. Eftekhar, A. Khelif, H. Moubchir, R. Westafer, W. D. Hunt, and A. Adibi, "Complete phononic bandgaps and bandgap maps in two-dimensional silicon phononic crystal plates," *Electron. Lett.*, vol. 43, no. 16, pp. 898–899, Aug. 2007.

[6] T. T. Wu, L. C. Wu, and Z. G. Huang, "Frequency band-gap measurement of two-dimensional air/silicon phononic crystals using layered slanted finger interdigital transducers," *J. Appl. Phys.*, vol. 97, no. 9, pp. 094916-1–094916-7, May 2005.

[7] I. El-Kady, R. H. Olsson, and J. G. Fleming, "Phononic band-gap crystals for radio frequency communications," *Appl. Phys. Lett.*, vol. 92, no. 23, pp. 233504-1–233504-3, Jun. 2008.

[8] F.-L. Hsiao, A. Khelif, H. Moubchir, A. Choujaa, C.-C. Chen, and V. Laude, "Waveguiding inside the complete band gap of a phononic crystal slab," *Phys. Rev. E, Stat. Phys. Plasmas Fluids Relat. Interdiscip. Top.*, vol. 76, no. 5, p. 056601, Nov. 2007.

[9] R. H. Olsson, I. F. El-Kady, M. F. Su, M. R. Tuck, and J. G. Fleming, "Microfabricated VHF acoustic crystals and waveguides," *Sens. Actuators A, Phys.*, vol. 145, pp. 87–93, Jul./Aug. 2008.

[10] N.-K. Kuo, C. Zuo, and G. Piazza, "Demonstration of inverse acoustic band gap structures in AlN and integration with piezoelectric contour mode wideband transducers," in *Proc. IEEE Int. Freq. Control Symp., Joint With 22nd Eur. Freq. Time Forum*, 2009, pp. 10–13.

[11] M. F. Su, R. H. Olsson, Z. C. Leseman, and I. El-Kady, "Realization of a phononic crystal operating at gigahertz frequencies," *Appl. Phys. Lett.*, vol. 96, no. 5, pp. 053111-1–053111-3, Feb. 2010.

[12] Y. M. Soliman, M. F. Su, Z. C. Leseman, C. M. Reinke, I. El-Kady, and R. H. Olsson, "Phononic crystals operating in the gigahertz range with extremely wide band gaps," *Appl. Phys. Lett.*, vol. 97, no. 19, pp. 193502-1–193502-3, Nov. 2010.

[13] A. Khelif, A. Choujaa, B. Djafari-Rouhani, M. Wilm, S. Ballandras, and V. Laude, "Trapping and guiding of acoustic waves by defect modes in a full-band-gap ultrasonic crystal," *Phys. Rev. B, Condens. Matter*, vol. 68, no. 21, p. 214301, Dec. 2003.

[14] A. Khelif, S. Mohammadi, A. A. Eftekhar, A. Adibi, and B. Aoubiza, "Acoustic confinement and waveguiding with a line-defect structure in phononic crystal slabs," *J. Appl. Phys.*, vol. 108, no. 8, pp. 084515-1–084515-5, Oct. 2010.

[15] S. Mohammadi, A. A. Eftekhar, W. D. Hunt, and A. Adibi, "High-Q micromechanical resonators in a two-dimensional phononic crystal slab," *Appl. Phys. Lett.*, vol. 94, no. 5, pp. 051906-1–051906-3, Feb. 2009.

[16] R. H. Olsson and I. El-Kady, "Microfabricated phononic crystal devices and applications," *Meas. Sci. Technol.*, vol. 20, no. 1, p. 012002, Jan. 2009.

[17] S. Pourkamali, G. K. Ho, and F. Ayazi, "Low-impedance VHF and UHF capacitive silicon bulk acoustic wave resonators—Part I: Concept and fabrication," *IEEE Trans. Electron Devices*, vol. 54, no. 8, pp. 2017–2023, Aug. 2007.